Selection of better mathematical model describing cake baking for inverse analysis

Puvikkarasan Jayapragasam, Pascal Le Bideau, Tahar Loulou

Selection of better mathematical model describing cake baking for inverse analysis

Puvikkarasan Jayapragasam, Pascal Le Bideau and Tahar Loulou*

Université de Bretagne Sud, Centre de Recherche, IRDL CNRS UMR 6027 F-56321, Lorient, France

tahar.loulou@univ-ubs.fr

November 21, 2020

Abstract

This paper presents selection criteria based on inverse solutions for mathematical models that predict heat and mass transfer involved in contact baking of cake. For the models in focus, the evaporation-condensation effect occurring during baking is incorporated by non-equilibrium (model - I) and equilibrium approach (model - II). Effect of product parameters on baking process is studied. To select an accurate model, weighted least square objective function and complex step differentiation method are employed. A numerical study with simulated measurements is performed to check the feasibility of parameter estimation from a single experiment. This numerical study showed that model II (i.e. with equilibrium approach) is more suitable for further inverse analysis. Significant weight given to temperature measurements resulted in better inverse solutions for both the models. Comparing final estimates from the models to the actual measurements, thermal properties approximated are close enough but mass transfer properties show deviations up to an order of magnitude. On extending the study for other baking conditions, it is found that inverse solution from model - II can adapt better than model - I for any change in the baking condition. Conclusively, a mechanistic model with equilibrium approach should be preferred than a model with explicit evaporation (model-I) for an inverse analysis. Eventually, this work aims to present an effective approach intended to resolve the challenges in accurate modeling of the baking process that arise due to limited knowledge of physical properties.

Keywords: Baking, Heat and Mass transfer, Non-dimensionalization, Parameter estimation

1 Introduction

Food processing largely owes the quality of its products to heat and mass transport taking place within the porous structure of the raw solid when in preparation. For instance in baking, texture and browness of the baked goods is influenced by physics of heat and mass transfer that manifests in chemical reactions like fermentation, volume

*Corresponding author

expansion of the porous dough, phase change with loss of moisture etc.; all these being strongly interconnected. Modeling of such complex transport phenomena in porous media can be broadly classified into three main families [1]: (1) Phenomenal approach [2–4], (2) Mechanistic approach [5–7] and (3) Semi-empirical approach [5, 8]. All the proposed models may include either transport phenomena [4,6,9–12] or structural mechanics [13,14] and sometimes both [3, 5, 7, 8]. The degree of non-linearity in these models increases with the number of phenomena that are taken into account. In all the categories mentioned above, the major difficulty is the lack of knowledge on transport properties to be used for modeling the baking process. These properties are mostly constants [7, 9], but sometimes can be functions of thermodynamic variables like temperature, moisture content, etc [4, 15]. Some authors have dedicated a lot of their work for estimating influential transport and rheological properties [7, 9, 15, 16]. The investigations are based on either indirect technique by solving inverse problems or direct technique by conducting specific experimental measurements.

This work focuses on modeling the baking process of a thick cake by direct heat conduction. It corresponds to cooking of bakery products on a hot pan like pancakes, crêpes. Mechanistic approach based on conservation of energy and mass is utilized to track the transport of individual phases inside the medium at macroscopic scale. One of the significant attributes is evaporation-condensation effect due to phase transition from liquid to vapor and vice-versa. It is responsible for liquid water migration towards crumb and transport of absorbed latent heat energy [17, 18]. Such effects are considered along with the inclusion of vapor phase in mathematical modeling. Generally, evaporation rate is formulated by explicit or implicit methods [19]. In explicit method [6], a specific expression for evaporation rate should be utilized while this is not required for implicit models that carry an inherent expression for it in the model [5, 8]. Some phenomenal methods [2, 3] are rarely used. Hitherto, there is no proper clarification about which approach is better, especially in food processing.

In this paper, the specific objectives are to (1) provide mechanistic models with both explicit and implicit approaches for a contact baking process in non-dimensional form; (2) identify the parameters that can be estimated through sensitivity analysis; (3) perform parameter estimation with synthetic (simulated profiles with presumed parameters) and experimental measurements and (4) identify which mathematical approach out of the presented ones is more suitable for solving the inverse problem and can be used in future work to approximate the influential thermophysical properties as functions.

Structure of the paper is as follows: Section 2 displays the governing equations for the models used, Section 3 presents experimental set-up, Section 4 details inverse procedure and finally Section 5 presents main results followed by conclusive remarks.

2 Mathematical model

Mechanistic approach is developed to predict temperature and moisture variations in the cake baking process. It is governed by conservation of energy and mass. The dough is cooked by placing on a hot surface maintained at a high temperature replicating domestic cooking over an electric or induction heating plate as shown in figure 1. The dough is sufficiently long along the x-axis that simplifies this problem to one dimensional form. Heat flux

($q(t)$) from cast iron floor enters the dough at the bottom boundary $x = o$, while the top surface is exposed to free convective heat (h_q) and mass (h_m) transfer.

[Figure 1 about here.]

The following assumptions are considered while formulating the mathematical model:

1. An effective mass diffusivity of liquid water is formulated that combines Fick's law of diffusion, capillary diffusion and even Soret effect (diffusion due to temperature gradient),
2. Continuum approach is utilized as it is difficult to formulate the complex porous structure and track the exact movement of the discrete phases [1],
3. Local thermal equilibrium exists between the phases and heat transfer due to convection and radiation inside the medium is negligible,
4. Heat and mass transport properties are constant and estimated as nondimensional numbers,
5. The gas in the medium is treated as ideal gas and obeys Dalton's law of partial pressure,
6. The effect of deformation is ignored which leads to no variation in solid phase (i.e. constant porosity).

Conflicts in modeling the evaporation rate: Water is present in both liquid and gaseous phase inside a hygroscopic material, a porous medium with large amount of bounded liquid water that deforms during drying. There are sufficiently large number of liquid water molecules present which can attain equilibrium instantly with the generation of few vapor bubbles during initial stage of baking. As temperature in the medium increases, the evaporation rate and generation of water vapor significantly increases. At a later stage, liquid water that is bound with solid might get inertia to attain equilibrium with water vapor. Hence, implicit evaporation rate with equilibrium assumption would not be a right choice. In such case, an explicit formulation with non-equilibrium approach would be much suited. Moreover, the models using equilibrium approach produced underestimation of core temperature with respect to experimental results [20] whereas with utilization of non-equilibrium approach, model with similar process functions produced better results [6]. Usually the non-equilibrium evaporation rate is linearly proportional to the difference between the actual vapor pressure in the medium and saturated vapor pressure [19].

There is no proper experimental validation for the above statement, creating a conflict whether liquid water attains equilibrium with vapor pressure or not [1]. This leads to the formulation of two different mathematical models in regard to evaporation rate described either by non-equilibrium approach [6, 19] or by equilibrium approach [5, 8]. In the remaining part of this paper, these two models are labeled as model I and model II, respectively. To make the paper self-contained, the governing equations for these two models are presented both in dimensional and nondimensional form in the following sections.

2.1 Governing equations in dimensional form

Fundamental mechanisms accountable for transport phenomena in a porous medium are molecular diffusion (for gases), capillary diffusion (for liquids), and convection (pressure driven or Darcy flow). The origin of governing equations are lies in conservation laws that are common for both the approaches [1]. The following equations are then transformed into required form for the respective models and are specified elaborately in the upcoming sections.

Mass conservation: The variations in water, vapor and air components during baking process are provided by following balance equations,

$$\frac{\partial (\rho_l S_l \pi)}{\partial t} + \nabla n_l = -I_v \qquad \text{for liquid water component} \tag{1}$$

$$\frac{\partial (\rho_v S_g \pi)}{\partial t} + \nabla n_v = I_v \qquad \text{for vapor water component} \tag{2}$$

$$\frac{\partial (\rho_a S_g \pi)}{\partial t} + \nabla n_a = 0 \qquad \text{for air component} \tag{3}$$

and completed by appropriate initial and boundary conditions detailed later in the paper.

Energy conservation: The energy conservation is written as,

$$\rho c_{p_{eff}} \frac{\partial T}{\partial t} = \frac{\partial}{\partial x}\left(k_{eff} \frac{\partial T}{\partial x}\right) - \lambda I_v \tag{4}$$

where $\rho c_{p_{eff}}$ and k_{eff} are effective thermal properties obtained by weighted addition of different components. The source term I_v will be detailed later in the upcoming sections. The above set of general equations (1)-(4) has been the starting point formany specialized studies that have modeled drying in porous media [1].

2.1.1 Boundary conditions:

There is no mass exchange at the contact plane between hot plate and dough ($x = 0$) and thus the flux for water (liquid and vapor together) and air is set to zero. On the other hand, there is significant heat transfer by conduction at this plane that initiates and drives the baking process. The incoming heat energy is modeled as time dependent heat flux ($q(t)$).

At free surface ($x = L$), the evaporated water present in respective volume fraction of liquid water and vapor are convected into the surroundings which is computed using convective mass transfer coefficient (h_m). Since at free surface the total gas pressure shall be same as ambient pressure, the remaining air pressure is computed as difference of ambient pressure and vapor pressure. These boundary conditions are expressed as:

$$n_l = 0 \qquad \text{at} \qquad x = 0 \tag{5}$$

$$n_l = h_m \pi S_l \left(\rho_v - \rho_v^{\infty}\right) \qquad \text{at} \qquad x = L \tag{6}$$

for liquid water component and

$$n_v = 0 \quad \text{at} \quad x = 0 \tag{7}$$

$$n_v = h_m \pi S_g \left(\rho_v - \rho_v^{\infty} \right) \quad \text{at} \quad x = L \tag{8}$$

for water vapor component,

$$n_a = 0 \quad \text{at} \quad x = 0 \tag{9}$$

$$\rho_a = \left(P_0 - P_v \right) / R_a T \quad \text{at} \quad x = L \tag{10}$$

for air component.

Similarly, energy transfer at the free surface, i.e. $x = L$, is expressed using a heat transfer coefficient (h_q). This coefficient combines convective and radiative heat transfers, and also accounts liberation of latent heat. The "pumping" condition at the surface due to excess gas pressure, as elobrated by Ni et al. [21], is ignored in the following formulations. These thermal boundary conditions are summarized by:

$$-k_{eff} \nabla T(x,t) = q(t) \quad \text{at} \quad x = 0 \tag{11}$$

$$-k_{eff} \nabla T(x,t) = h_q \left(T(x,t) - T^{\infty} \right) \quad \text{at} \quad x = L \tag{12}$$

2.1.2 Model I

Model I is formulated with evaporation rate based on non-equilibrium assumption. The balance equations described above are applicable for this model except the mass conservation of liquid water, expressed slightly different from equation (1) and is written as:

$$\rho_s^a \frac{\partial U}{\partial t} + \nabla n_l = -I_v \tag{13}$$

Where U is moisture content on dry basis defined as the ratio of liquid water density to solid density, (i.e. ρ^a ρ_g^a), and mass flux (n_l) for highly saturated porous media with very low liquid permeability can be simplified by Fick's law [5, 8].

$$n_l = -D_l \rho_s^a \left(\nabla U \right) \tag{14}$$

For gas phase, mass flux for water vapor (n_v) and air (n_a) is defined by Fick's law for binary diffusion and pressure gradient by Darcy's law and is written as [22]:

$$n_v = -\rho_v \frac{k_g}{\mu_g} \nabla P_g - D \rho_g \nabla \left(\frac{\rho_v}{\rho_g} \right) \tag{15}$$

$$n_a = -\rho_a \frac{k_g}{\mu_g} \nabla P_g - D \rho_g \nabla \left(\frac{\rho_a}{\rho_g} \right) \tag{16}$$

Modeling source term I_v : The evaporation rate in this model is framed as linear difference between actual vapor pressure and saturated vapor pressure and given by,

$$I_v = H\left(\rho_v^{eq} - \rho_v\right) \tag{17}$$

where H denotes the evaporation rate constant. With the help of saturated vapor pressure (P_{sat}) and water activity (a_w) [5, 7, 8, 16, 23], equilibrium vapor density ρ^{eq} is estimated by the following expression:

$$\rho_v^{eq} = a_w(T,U) \cdot P_{sat}(T) \Big/ \left(R_v T\right) \tag{18}$$

2.1.3 Model II

This model accounts for evaporation through the equilibrium approach. It implies that the actual vapor pressure inside the medium is equated to equilibrium vapor pressure. The balance equations are simplified and combined in this model. The source/sink term in liquid water (moisture content, equation (1)) is replaced by water vapor conservation (equation (2)). The moisture content is stated by,

$$\rho_s^a \frac{\partial U}{\partial t} + \frac{\pi P_v}{R_v T}\frac{\partial S_g}{\partial t} - \frac{\pi S_g P_v}{R_v T^2}\frac{\partial T}{\partial t} + \frac{\pi S_g}{R_v T}\frac{\partial P_v}{\partial t} = \nabla\cdot\underbrace{\rho^a D_s \nabla U + \frac{\rho_v k_g}{\mu_g}\nabla P_g + \rho_g D_v \nabla \frac{\rho_v}{\rho_g}}_{\Gamma} \tag{19}$$

Based on ideal gas law, the air conservation equation is transformed to define air pressure as,

$$\frac{\partial}{\partial t}\left(\frac{\pi S_g P_a}{R_a T}\right) + \nabla\cdot n_a = 0 \tag{20}$$

From the above expression, total gas pressure is stated by Dalton's law of partial pressure ($P_a = P_g - P_v$) as,

$$\frac{\pi}{R_a}\left(\frac{S_g}{T}\frac{\partial P_g}{\partial t} - \frac{S_g P_g}{T^2}\frac{\partial T}{\partial t} + \frac{P_g}{T}\frac{\partial S_g}{\partial t}\right) + VP + AP + BP = 0 \tag{21}$$

where the variables VP, AP and BP are defined by:

$$VP = -\frac{\pi}{R_a}\left(\frac{S_g}{T}\frac{\partial P_v}{\partial t} - \frac{S_g P_v}{T^2}\frac{\partial T}{\partial t} + \frac{P_v}{T}\frac{\partial S_g}{\partial t}\right)$$

$$AP = -\nabla\cdot\left(\frac{P_g k_g}{R_a T \mu_g}\nabla P_g - \frac{P_v k_g}{R_a T \mu_g}\nabla P_g\right)$$

$$BP = \nabla\cdot\left(\frac{1}{T}\left(\frac{P_v}{R_v} + \frac{P_g - P_v}{R_a}\right) D_v \times \nabla\left(\frac{\left(1\right)}{1 + \frac{P_g - P_v}{P_v}\frac{R_v}{R_a}}\right)\right)$$

The closure evaporation term for energy balance equation is directly computed from water vapor conservation as given by equation (2). In above equations, gas densities are expressed in form of pressure for convenience in solving the equations.

Boundary condition The boundary condition are similar to those of the previous model. Since these equations appear in combined form, the boundary conditions are also simplified as

$$\Gamma = 0 \quad \text{at} \quad x = 0 \tag{22}$$

$$\Gamma = h_m \left(\rho_v - \rho_v^{\infty} \right) \quad \text{at} \quad x = L \tag{23}$$

for the moisture content

$$\nabla P_g = 0 \quad \text{at} \quad x = 0 \tag{24}$$

$$P_g = P_0 \quad \text{at} \quad x = L \tag{25}$$

for total gas pressure.

Finally, in the equilibrium approach, energy equation remains same as given by equation (4) and will be solved with the same boundary conditions (11) and (12).

2.2 Governing equation in nondimensional form

In many engineering problems, the difference in order of magnitude between the dimensional parameters and/or functions are quite large and therefore making these parameters extremely unwieldy. Consequently, mathematical modeling, computations and presentation of the results are also cumbersome. Normalization may be used to arrange these unknown quantities as nondimensional groups and simplify drastically the mathematics and presentation of the results.

For the sake of brevity, the intermediate steps for converting these governing equations into nondimensional form are elaborated in appendix A and their final form for both the models are presented in table 1.

[Table 1 about here.]

The analytic expressions of the two variables Γ and Φ, displayed in table 1, are given by:

$$\Gamma = D_l^+ \nabla U + \frac{a_p^+ V}{\pi S_g} \nabla P_g^+ + \frac{\rho_{ref}^+}{1+\theta} \left(P_g^+ - P_v^+ \left(1 - 1/R_v^+ \right) \right) D_v^+ \nabla \left(\frac{1}{1 + R_v^+ P_g^+ / P_v^+ - 1} \right)$$

and

$$\Phi = \frac{\left(P_g^+ - P_v^+ \left(1 - 1/R_v^+ \right) \right) \rho_{ref}^+ D_v^+}{1+\theta} \nabla \left(\frac{1}{1 + R_v^+ P_g^+ / P_v^+ - 1} \right) - \nabla \left(\frac{\left(P_g^+ - P_v^+ \right) a_p^+ \rho_{ref}^+}{1+\theta} \nabla P_g^+ \right)$$

respectively.

The unfamiliar dimensionless numbers appearing in those equations are summarized in table 2. The normalization procedure created these sets of dimensionless parameters $\Omega_1 = \left[a_q^+, Bi_q, D_l^+, D_v^+, H^+, k^+ \right]$ for model I and $\Omega_2 = \left[a_q^+, Bi_q, D_l^+, D_v^+, k^+ \right]$ for model II. As a result of the normalization process, the number of unknowns present in the initial physical problem have been reduced and the knowledge of these two sets is sufficient to describe the baking process efficiently for both the cases. Dimensionless time is usually defined as Fourier number which has diffusivity term in it. Since this diffusivity term is unknown and meant to be found, it would not be a right choice to define nondimensional time as Fourier number and thus leads to development of these unfamiliar parameters.

[Table 2 about here.]

The mathematical models described so far constitute the direct problem in dimensionless form for both model I and II. The temperature and moisture variations are calculated after defining geometry, initial and boundary conditions and thermophysical properties. Heat and mass transfer problems are highly nonlinear and are solved by numerical tools in almost all cases (finite difference, finite elements, hybrid methods, . . .). In the present study, the Comsol® software [24] is used to solve the problem under investigation.

3 Experimental device

A detailed description of experimentation of the baking process has been explained in previous works [25, 26]. However, to make the paper self-contained, a short description of experimental procedure is presented here. The entire experimental setup is shown schematically in figure 1. A heating coil whose temperature can be regulated through relay has been used as heating source. In this work, the regulator temperature is maintained at 200°C for all the case studies. This heating coil was placed below a cast-iron disk measuring 23 cm in diameter and 2 cm in height. The iron disk was chosen with high thermal conductivity to ensure homogeneous temperature distribution in its radial direction. The lateral sides of heating coil and cast iron disk were insulated to avoid heat losses and the complete assembly was placed on a high precision balance.

The weighing balance (Manufacture: Radwag®, model: PS6000R2) was used to record the overall mass variation during baking. This kind of balance uses the most advanced technique allowing measurement with the readability of 0.01 g and maximum capacity of 6 kg. Its exclusive technology guarantees repeatability over the whole experimental life cycle and also ensures high resistance to ambient conditions change (temperature, humidity, . . .).

The batter sample was prepared by mixing an industrial mix (commercial name Francine ®) containing wheat flour, corn flour and eggs with milk in mass proportion of 3 : 5. A bottomless polytetrafluoroethylene (PTFE) mold of dimensions $14 \times 11.5 \times 2$ (W × B × H in cm) was used for two purposes. First, as a support for the dough during initial stage due to its high moisture content and second, to house many thermocouples (Tc_3, Tc_4, Tc_5) for temperature measurements at different locations $0 < x_1, \ldots x_i \ldots, < L$. In the present work, two K-type thermocouples (made locally in our laboratory) are used at 0.1 mm (Tc_3) and 4 mm (Tc_4) away from cast-iron disk/dough interface. An optical pyrometer (Tc_6, Manufacturer : Optris, model: CS LT), i.e. a non-contact method of temperature measurement, recorded the surface temperature by setting the dough emissivity to 0.9. This kind of sensor is easy to install and has less measurement noise. Since volume deformation is noted during baking operation, the position and location of sensors should be ensured as their measurements are input for the inverse problems. In order to ensure the firmness in position of sensors during deformation of dough, the either ends of thermocouples are stretched passed through pre-drilled holes in the mold. After baking process, the dough is bisected to locate the position of the thermocouples and was found that their positions were unaltered. The measurement of non-contact optical pyrometer and mass variations for moisture content are independent of deformation. Thus, neglecting deformation effect in mathematical modeling shall not have major influence in the inverse solution.

All temperature measurements were recorded using unique data acquisition system (Manufacturer: HBM, model : Quantum X MX1609) with the sampling rate of 50 Hz, i.e measurement recorded at each time step of $\Delta t_m = 0.02$ s. The baking process was carried out for period of approximately 20 min. The water activity used in this work was an approximation of isotherm curve expressed by Ferro-Fontan relation [26, 27].

4 Inverse problem formulation

In this paper, the inverse problem is aimed to estimate the two sets of parameters $\Omega_1 = [a_q^+, Bi_q, D_l^+, D_v^+, k^+]$ in model I and $\Omega_2 = [a_q^+, Bi_q, D_l^+, D_v^+, k^+]$ in model II. Looking at these models, the number of parameters to be estimated are reduced in model II due to assumption of equilibrium approach.

In nutshell, the aspiration of an inverse problem is to minimize cost or objective function that is built as squared differences between measurements and model responses (computed temperature and moisture content). Gradient based optimization methods are well suited and extensively used for minimizing the objective function. In this study, optimization problem is solved using a inbuilt lsqnonlin function [28,29] from Matlab software [30]. The components in the cost functions are Euclidean distance of temperature and mean moisture content between measurements and simulated results.

The order in magnitude between temperature and moisture content in nondimensional form is different and also the wealth of information brought by each kind of measurement differs substantially. With these discrepancies, objective function based on ordinary least square (OLS) method may not result in desired output for either temperature or moisture content in comparison with measurements. To overcome this difficulty, objective functions like weighted least square, scaled least square, etc., are used to balance the contribution from each kind of measurements [31]. Weighted least square (WLS) objective function as defined in equation (26) is used here.

$$S_{WLS} = \varphi\,(\mathbf{M}_\theta - \mathbf{E}_\theta)^\top (\mathbf{M}_\theta - \mathbf{E}_\theta) + (1-\varphi)\,(\mathbf{M}_U - \mathbf{E}_U)^\top (\mathbf{M}_U - \mathbf{E}_U) \tag{26}$$

where S_{WLS} is the objective function to be minimized, $\mathbf{M}$ and $\mathbf{E}$ stand for measured values and estimated values respectively. Herein, $\mathbf{E}$ and $\mathbf{M}$ are column vectors with temperature and mean moisture content variables arranged in similar fashion. The column vector for estimated values $\mathbf{E}$ for temperature and moisture content are given as,

$$\mathbf{E}_\theta = [\theta_1^1, \theta_2^1, \cdots, \theta_{N_t}^1, \cdots, \theta_1^{N_\theta}, \theta_2^{N_\theta}, \cdots, \theta_{N_t}^{N_\theta}]^\top \quad \text{and} \quad \mathbf{E}_U = [U_1, U_2, \cdots, U_{N_t}]^\top$$

Here N_t refers to number of transient measurements, N_θ represents the number of temperature sensors installed inside the dough. As shown in equation (26), S_{WLS} is weighted objective function with two different weight factors, φ for temperature and $1-\varphi$ for moisture. By doing so, a better estimation is accomplished by weighting the contribution of each kind of measurement.

Sensitivity coefficients or Jacobian matrix elements, $X_k^F(i)$, are required for the sensitivity analysis and minimization of cost function S_{WLS}. In general, these sensitivity coefficients are computed by simple and convenient Finite Difference Method (FDM) but this method suffers from rounding-off error, truncation error, step-size dilemma due to subtraction operation, etc and also requires $2n_p + 1$ computational runs in case of central FDM for n_p number

of parameters. In order to overcome such unavoidable errors, complex step differentiation method (CSD) [32, 33] is implemented for sensitivity computation. CSD is derived from Taylor series expansion of a function with complex step interval jh about a point x as,

$$f(x + jh) = f(x) + jhf'(x) - h^2\frac{f''(x)}{2!} - jh^3\frac{f'''(x)}{3!} + \cdots$$

With focus on first derivative, the above Taylor series expansion is modified by taking imaginary part yields,

$$f'(x) = \frac{\mathrm{Im}[f(x + jh)]}{h} + h^2\frac{f'''(x)}{3!} + \cdots$$

This equation is used for sensitivity computation with approximation of $O(h^2)$ that estimates first derivative of function $f(x)$ which is in same order as central Finite Difference Method but requires lesser number of computational runs. With advantage of handling complex variables in Matlab-Comsol environment, sensitivity coefficients for the models with respect to parameter vectors Ω_i is computed as,

$$X_k^F(i) = \frac{\partial F(\Omega_k(i))}{\partial \Omega_k(i)} = \frac{\mathrm{Im}\left[F(\Omega_k(1), \ldots \Omega_k(i) + jh, \ldots, \Omega_k(N_{p_k}))\right]}{h} \tag{27}$$

where i varies from 1 to N_{p_k}, Im is a function which returns the imaginary part of a complex number, j is complex number ($j^2 = -1$), i is i^{th} component of the vector Ω_k, N_{p_k} is number of component in vector Ω_k, F is either of state variables (θ or U) and k is either 1 for model I or 2 for model II. For detailed explanation about executing CSD in Matlab for a heat transfer problem can be understood from literature [33].

Correlation between the parameters of each vector Ω_k, $k = 1, 2$ can be obtained using the covariance matrix of parameters [34]. The ij element of the correlation matrix is given by

$$r_{ij} = C\left(\Omega_k(i), \Omega_k(j)\right) = \frac{\mathrm{cov}(\Omega_k(i), \Omega_k(j))}{\sqrt{\mathrm{var}(\Omega_k(i))\mathrm{var}(\Omega_k(j))}} \tag{28}$$

In equation (28), $\mathrm{cov}(\Omega_k(i), \Omega_k(j))$ is the co-variance of the Jacobian matrix ($\mathbf{X}$) between the parameters $\Omega_k(i)$ and $\Omega_k(j)$ and $\mathrm{var}(\Omega_k(i))$ is the variance of the Jacobian matrix ($\mathbf{X}$) for parameter $\Omega_k(i)$. The diagonal elements of $\mathbf{r}$ are unity and the off-diagonal element must be in the interval $[-1, 1]$. Whenever all the off-diagonal elements exceed the absolute value 0.9, then the estimates tend to be correlated and become inaccurate.

5 Results and discussions

[Table 3 about here.]

In this work, the governing equations for the models (forward problem) are solved in Comsol [24] using 3 or 4 General forms PDE from Mathematics module with subcategory PDE Interfaces, depending upon number of required governing equations to be solved. With help of Flux/Source option for boundary condition, the incoming heat flux is applied for energy conservation PDE which replicates the heat transfer from the cast iron floor. The inverse problems (optimization) are carried out in Matlab [30] using built-in *lsqnonlin* function. In Sensitivity analysis of transport properties is performed to identify parameters that result create the least variation in measured

state variables. These identified parameters along with other available properties from literature are imposed in forward problem while solving the inverse problem for the models (see table 3). For instance, convective mass transfer coefficient or Biot number for mass transfer (Bi_m) can be expressed using Biot number for heat transfer (Bi_q) and fluid properties. Similarly, the parameter (R_l), which is the product of density ratio and Jakob's number, can also be derived since latent heat of vaporization (λ) and other variables are known.

The simulated temperature and mean moisture content profiles for model II using transport properties given in table 3 are shown in figure 2. Three temperature sensors located at $x = 0$ mm, $x = 4$ mm and $x = 8$ mm, are used for simulations. For moisture content, spatial averaged weight loss during the baking process is considered to be recorded.

[Figure 2 about here.]

5.1 Sensitivity analysis

The parameters required for sensitivity analysis are derived as mean value from literature [5, 8] and are shown in table 3. Since the scaled sensitivity profiles for temperature are almost similar at different location of sensors, only sensor location at free surface $x^+ = 1$ are presented graphically for both the models.

Figure 3 presents overview of scaled sensitivity for both the models. For model I, only thermal properties like thermal conductivity (k^+), diffusivity (a_q^+) and Biot number (Bi_q) are found sensitive with respect to temperature (see figure 3a) while mass transfer properties (D_l^+, D_v^+) and evaporation rate (H^+) are sensitive with respect to mean moisture content (see figure 3c).

[Figure 3 about here.]

In comparison to previous model with explicit evaporation rate, model II produces better sensitivity for mass diffusivities of liquid water (D_l^+) and water vapor (D_v^+) with respect to temperature (see figure 3b), thus indicating that implicit evaporation rate can result preferable approximation as the mass transfer properties (D_l^+, D_v^+) are sensitive to both temperature and mean moisture content. The overview of these scaled sensitivity analysis indicate that:

1. Only parameters concerning with thermal properties like thermal conductivity (k^+), thermal diffusivity (a_q^+), Biot number (Bi_q) are sensitive with respect to temperature for explicit evaporation, while other parameters are least sensitive,
2. The parameter (a_p^+) derived from permeability shows least sensitivity stipulating that it would be a tedious task for estimation of this parameter using gradient based optimization,
3. Magnitude of sensitivity with respect to mean moisture content may be reduced due to spatial averaging. If local measurements were used, they would have shown higher sensitivity,
4. Implicit evaporation approach (model II) might result in better inverse solution than explicit evaporation approach because apart from thermal properties, parameters of mass transfer like mass diffusivity of liquid water and water vapor are sensitive with respect to temperature.

The sensitivity analysis for porosity (π) and capillary diffusivity (a_p^+) are also performed. It is found that the capillary diffusivity between the range 10^2 and 10^4, has no major impact on temperature and mean moisture content profiles. Similarly, the impact due to variation of porosity is also insignificant and it might be due to the assumption of constant porosity and no deformation. Very poor sensitivity for all the parameters is observed with respect to pressure for both the models and hence is not presented here. Therefore, consideration of state variable pressure in inverse problem as one of the elements in Jacobian matrix (J) and cost function (S) will not improvise the solution in any manner.

5.2 Inverse solution from synthetic measurements

For the sake of surety, the inverse analysis are executed by simulated or synthetic measurements before using it with actual experimental data, i.e., the simulated temperature and mean moisture content profiles based on non-dimensional parameters displayed in table 3 is employed as experimental measurements. If these models are successful in this trial, actual experimental data will be used later for inverse solution. This increases reliability of the final inverse solution. In the following text, "exact ones" indicates the unaltered simulated temperature and mean moisture content profiles which are different from experimental measurements. In order to reduce the correlation between the forward problem employed in inverse solution and the synthetic measurement, some randomness in these simulated profiles are added by inclusion of random variable.

The noise in the measurements are added to the exact profiles as following,

$$\theta(x, t) = \theta_x(x, t) + \omega\sigma_\theta \tag{29a}$$

$$U(t) = U_x(t) + \omega\sigma_U \tag{29b}$$

where $\theta(x, t)$ and $U(t)$ are simulated measurements containing random errors, $\theta_x(x, t)$ and $U_x(t)$ represent exact profiles obtained with known parameters, σ_θ and σ_U are standard deviation of measurement errors and ω is random variable with normal distribution, zero mean and unitary standard deviation. The standard deviations of temperature and moisture content are chosen as some percentage to its maximum and given by $\sigma_\theta = 1.0\% \times \theta_{max}$ and $\sigma_U = 1.0\% \times U_{max}$ respectively.

Model I: Before proceeding to the estimation procedure, a check for linear dependency between the parameters are performed with help of correlation matrix tabulated in table 4. This matrix shows that only thermal conductivity k^+ and thermal diffusivity a_q^+ are dependent while others are not.

[Table 4 about here.]

[Table 5 about here.]

Table 5 gives an idea about relative percentage error of estimated parameters with respect to exact ones for model I. The result shows irrespective of weighting factor, mass transfer properties (D_l^+, D_v^+) and Biot number (Bi_q) have error more than 5%. This implies that only thermal properties like conductivity (k^+), diffusivity (a_q^+) and evaporation rate constant (H^+) can be estimated with high accuracy.

Model II: On looking at the correlation matrix in the table 4, almost all the parameters are dependent on each other expect Biot number (Bi_q). This might affect efficiency of the inverse problem for this model. The percentage error for the estimated parameters with respect to exact ones can be seen from table 5.

Despite of correlation for most of the parameters, it is visible that this implicit evaporation rate model facilitates the inverse problem in simultaneous estimation of thermal and mass transfer properties. The percentage errors for simulated data with $\sigma = 0$ and $\varphi = 0.5$ are least implying that information from temperature and moisture content are equally important. Considering simulated data with noise, some parameters show minimal relative error for $\varphi = 0.4$ and some for $\varphi = 0.6$ but again the weighting factor $\varphi = 0.5$ have a balanced result.
Simultaneously estimation of the parameter vectors $\Omega_{1,2}$ is feasible for both the models. But these models have some trouble in retrieval of certain parameters especially mass transfer properties, which are stipulated by larger relative errors in the table 5. Out of these two models, model I has shown bigger errors for parameters $D^{\star}_{w}, D^{\star}_{v}$ and this is mainly due to weak sensitivities of temperature with respect to these parameters while compared with results from other model. Though model I has least correlation among parameters, at any given weight φ and parameter, model II has better estimation than model I. Hence, it is preferable to consider model II with implicit method for parameter estimation.

5.3 Estimated parameters with experimental data

Inverse problem is extended further with measured temperature and moisture content profiles obtained by experimental setup described in section 3. These experimental profiles can be perceived from figures 4, 5 which are presented as symbols.

Model I: The components in vector Ω_1 are estimated without any difficulties for any weighting factor ($\varphi = 0.4, 0.5$ and 0.6). Table 6 generalizes the following outcomes from the inverse solutions for different weighing factors:

- Thermal properties such as conductivity (k^+), diffusivity (a_q^+) and Biot number (Bi_q) are almost consistent,
- Mass diffusivity (D_w^+) for liquid water for the weighting factor $\varphi = 0.6$ seems to be doubled from other two factors. Mass diffusivity (D_v^+) between water vapor and air has huge variations for different factors and increases with increasing weighting factor. Such large variation is obvious due to least sensitivity of this parameter with respect to temperature (see figure 3),
- The trends of evaporation rate (H^+) decreases with increasing value of φ.

[Figure 4 about here.]

It is a difficult to sort out the better inverse solution among the presented ones from the table 6. Therefore, a quick comparison of rms values for temperature and moisture content profiles with experimental measurements is carried out from the table 7. Weighting factor $\varphi = 0.6$ is observed to have minimal errors among all factors. Graphical deviation of estimated profiles, using inverse solution with $\varphi = 0.6$, from measured data are showcased in figure 4. Estimated temperature profiles almost follow similar trends with measurements for thermocouples Tc4 and Tc6 but

temperature for Tc3 shows small discrepancy after 1000 seconds of baking time. Estimated mean moisture content in comparison to measurements show an underestimation of mass loss for almost first half of baking period but eventually ended with the value close enough to the observation.

[Table 6 about here.]

[Table 7 about here.]

Model II: Parameter vector Ω_2 from model II is approximated using measured data for various weighing factors. A consistency in estimated parameters can be seen from table 6. A detailed examination show that the only parameter with maximum variation (up to 21%) among the weighing factors is D_v^+ while thermal properties like a_q^+, k^+ showed minimal variations (up to 5%). Rms error comparison is also utilized in this case to pick up the better inverse solution from table 6.

[Figure 5 about here.]

Table 7 gives an overview of rms error between estimated and measured profiles at different sensor locations for three weighing factors (φ = 0.4, 0.5 and 0.6). Inverse solution with weighing factor φ = 0.6 seems to be better due to its overall least rms errors among others. Figure 5 gives an insight on behaviors of temperature and moisture content profiles simulated using inverse solution in collation with measurement profiles. Mean moisture content follows almost exactly the same trend with measured values while temperature especially for thermocouple Tc3 is in contrast with observation.

[Table 8 about here.]

Inverse solutions of parameter approximation in dimensional form for both models with weighting factor φ = 0.6 are tabulated in table 8 and following inferences are concluded:

- Thermal properties such as conductivity (k_{eff}), volumetric heat capacity ($\rho c_{p_{eff}}$) and convective transfer coefficient (h_q) are almost equivalent for both the models and lie within the range of nominal values presented in literature [35],
- Model I is able to predict liquid water diffusivity (D_w) close to the value stated in literature [5] whereas model II estimated an order less. Mass diffusivity (D_v) of water vapor from model I is closer to binary diffusion coefficient between vapor and air. But due to tortuous structure this estimated value should be slightly lower than normal as seen in model II estimation. Higher mass diffusivities in model I may be due to lower evaporation rate at the region near cast iron disk/dough interface and mass loss is only escalated by mass transfer at ambient interface. To compensate mean moisture loss, diffusivities have been estimated little higher facilitating mass diffusion and loss through convection into ambient for model I. The reason behind it can be owing to use of constant evaporation rate,
- The nominal range of evaporation rate for water vapor found around 1 (1/s) [6, 36]. Such value is achieved only for φ = 0.6 and not for other weighting values (when converted in dimensional form),

- Looking into estimated profiles from figure 4 and 5, model I seems to replicate measurement values for temperatures but model II has better approximated mean moisture content.

5.3.1 Validation of inverse solutions

All the above presented inverse solutions are derived from measurements performed with heating coil temperature regulated at 200°C. But in order to validate the inverse solutions, the solution is extended to another regulator temperature of 170°C. The only difference from the previous experimental set-up is the incoming heat flux at the interface between cast-iron floor and dough which are formulated by a mathematical expression as function of baking time, $q(t) = 22700 \times t^{-0.36}$. As expected the magnitude of the heat flux has been reduced as the temperature of heating coil is also reduced. The inverse procedure for heat flux estimation can be found in literature [25] and not presented in detail here for sake of brevity. With the estimated parameters and the current heat flux function, the temperature and mean moisture content are simulated and compared with the experimental measurements. During measurement, the thermocouple T4 has been misplaced and came in contact with the cast-iron floor which gave inaccurate readings and are not as accurate as previous study.

[Figure 6 about here.]

Figure 6 gives graphical comparison of measurement and simulation preformed from estimated parameters for model I and II with regulator temperature at 170°C. On analysis, except temperature at T4, both the models produce desirable results for temperature and mean moisture content. The moisture content at end of baking is 1.35 [kg/kg dm] for the baking with current regulator temperature whereas it was 1.32 in previous studies. The simulation of model I ended up with value of 1.36 for mean moisture content at baking time of 20 minutes and model II with 1.35. The mass loss of model II were close enough to experiment and have similar trends alike earlier simulation indicating that those estimated parameters are capable of reproducing simulation for other baking conditions. Whereas in case of model I, the profile was similar but the mass loss at end of baking were overestimated in former study and slightly underestimated in present one. These stipulate that any one the estimated parameters especially related to mass transfer did not compete with other baking conditions. The possible parameters that causes some difference are mass diffusivities $D_w^\star$, $D_v^\star$, convective mass transfer coefficient appearing at boundary condition Bi_m and evaporation rate constant $H^\star$. Since mean value for moisture content is used, the change in diffusivities would have affected local moisture content but not the average one. Hence any variation in the mass diffusivities would not strongly influence the simulated results. The another possibility is due to mass transfer coefficient which is derived from convective heat transfer coefficient. But by observing the temperature profile at sensor location T6, simulation and measurement almost merge with each other (see figure 6(a)) implying that the boundary condition from estimated are adequate and does not require any modification. So the only option left is evaporation rate which is a generic value prove here that it should be estimated for each experimental set-up.

6 Conclusion

One-dimensional models describing heat and mass transfer during one sided baking of cake are proposed and compared. A complete overview and comparison of estimated parameters between two such models: explicit with non-equilibrium approach (model I) and implicit with equilibrium approach (model II) for evaporation rate in baking process is performed from synthetic and experimental data. Deformation effect is not included since there is no generation of gases like carbon dioxide expect water vapor due to evaporation phenomenon.

The proposed mathematical models are converted in nondimensional form to bring out the key parameters governing the baking process. The effectiveness of inverse problem is enhanced using complex step differentiation for computing the elements of the Jacobian matrix. The sensitivity analysis performed over process parameters has shown that the capillary diffusivity (a_p^+) derived based on permeability would be difficult to be estimated accurately. Indeed, linear dependency among the parameters to be estimated simultaneously in these two models is examined and shows that model I has the least dependency due to its explicit evaporation approach.

The comparison of these two models is based on accuracy of inverse solution with synthetic data. It has shown that model II is much suited as the relative errors between exact and estimated parameters are the lowest. Looking at the rms values of temperature and moisture content profiles between simulated and estimated ones, model II produces minimal values compared to model I. This is due to poor sensitivity of mass transfer properties for model I which has widen the confidence interval.

Finally, explicit model and implicit model are tested with the same experimental data obtained locally with a dedicated experimental setup. The inverse solution gives almost the same thermal properties values (thermal conductivity and specific heat) for both models and the value of heat transfer convection coefficient is found to be more important for model I than model II. The estimated liquid water and vapor diffusivities are found one order greater for model I. In comparison with available literature data, model I tends to overestimate the physical parameters driving the baking process.

The extension of inverse solution for other baking conditions also imply that the model with implicit approach (model-II) is much suited for estimation of properties using inverse problems. This analysis also proves the point that the evaporation rate in model-I is different and should be estimated for each experimental conditions individually. From this paper, it can be concluded that model-II is much better than the model - I with explicit evaporation rate for inverse analysis which can used for estimation of properties, evaluating optimal heat input, etc.

Since the boundary condition is of second kind with non-zero heat flux, uniqueness in solutions from inverse problems for the models can be excepted. The implemented input parameters are either measured or derived by experimental measurements like heat flux, water activity that makes more reliable on the parameter estimations. Another point to mention is that searching for the best model to represent the baking process is still under progress in food engineering community. When a such model has been identified, the inverse analysis will suffer lesser from the inherent uncertainties of the input data.

Since the transport properties are assumed as constants, it has terribly failed in accounting the crust-crumb transformation from dough. This factor is reflected on model II for simulated temperature profiles at sensor location T3 which did not show a linear increase after a plateau at 100°C. Further work is under progress to account such

phenomenon and may give more insights about the first drawn conclusions presented in this paper.

Acknowledgements

The authors are grateful for the research funding provided by the Brittany Region (Région de Bretagne, France) (ARED financial support).

Conflict of interest

The authors declare that they have no conflict of interest with any people or organisations about this work.

Nomenclature

Latin Letters

a_w Water activity

c_p Specific heat capacity, [J/(kg · K)]

D Mass diffusivity with index, [m^2/s]

E Estimated value

H Evaporation rate constant, [1/s]

h_m Convective mass transfer, [m/s]

h_q Convective heat transfer, [W/(m^2 · K)]

I_v Evaporation rate, [kg/(m^3 · s)]

X Jacobian matrix

k Thermal conductivity, [W/(m · K)]

k permeability, [m^2]

M Measured value

n Mass flux with index, [kg/(m^2 · s)]

P Pressure, [Pa]

q Applied heat flux, [W/m^2]

R_i Specific gas constant of species i, [J/(kg · K)]

S Objective function

S Saturation

T Temperature, [K]

t Time, [s]

$\bar{U}$ Mean moisture content

U Moisture content, [kg of liquid/kg of solid]

x location, [m]

Greek Letters

ρ Density, [kg/m^3]

λ Latent heat of vaporization, [J / kg]

μ Dynamic Viscosity, [Pa · s]

N_θ number of temperature sensor

N_t number of transient measurements

Ω_i Parameter vector

$|\cdot|$ Euclidean norm

φ weighting factor

π Porosity

Non dimensional numbers

A Air density

a_p^+ Capillary diffusivity

a_q^+ Thermal diffusivity

Bi_q Biot number for heat transfer

Bi_m Biot number for mass transfer

D_l^+ Liquid water diffusivity

D_v^+ Vapor diffusivity

G Total gas density

H^+ Evaporation rate constant

I_v^+ Evaporation rate

k^+ Thermal conductivity

P_g^+ Total gas pressure

P_v^+ Vapor pressure

Q Applied heat flux

R_l product of density ratio and Jacob's number

ρ_{ref}^+ Reference density

R_v^+ ratio of gas constants of vapor and air

θ Temperature

V Vapor density

Abbreviations

CSD Complex Step Differentiation

DOE Design Of Experiments

FDM Finite Difference Methods

OLS Ordinary least square

WLS Weighted least square

Superscripts

a apparent

∞ Ambient

⊤ Transpose

Subscripts

a air

eq Equilibrium

eff effective

f final

g total gas

o Initial Value

l liquid

s solid

sat Saturated

v vapor

References

[1] A.K. Datta. Porous media approaches to studying simultaneous heat and mass transfer in food processes I: Problem formulations. *Journal of Food Engineering*, 80:80–95, 2007.

[2] I. Zheleva and V. Kamburova. *Predictive Modeling and Risk Assessment*, chapter Modeling of Heating During Food Processing, pages 79–99. Springer, Boston, MA, 2009.

[3] B. Zanoni, S. Pierucci, and C. Peri. Study of the bread baking process - ii. mathematical modelling. *Journal of Food Engineering*, 23(3):321–336, 1994.

[4] K. Thorvaldsson and H. Janestad. A model for simultaneous heat, water and vapour diffusion. *Journal of Food Engineering*, 40(3):167–172, 1999.

[5] J. Zhang and A.K. Datta. Mathematical modeling of bread baking process. *Journal of Food Engineering*, 75:78–89, 2006.

[6] Ousegui A., Moresoli C., Dostie M., and Marcos B. Porous multiphase approach for baking process – explicit formulation of evaporation rate. *Journal of Food Engineering*, 100(3):535–544, 2010.

[7] M. Lostie, R. Peczalski, J. Andrieu, and M. Laurent. Study of sponge cake batter baking process. ii. modeling and parameter estimation. *Journal of Food Engineering*, 55(4):349–357, 2002.

[8] V. Nicolas, P. Salagnac, P. Glouannec, J.P. Ploteau, V. Jury, and L. Boillereaux. Modeling heat and mass transfer in deformable porous media: Application to bread making. *Journal of Food Engineering*, 130:23–35, 2014.

[9] E. Purlis and V.O. Salvadori. Bread baking as a moving boundary problem. part 2: Model validation and numerical simulation. *Journal of Food Engineering*, 91:434–442, 2009.

[10] Emmanuel Purlis and Viviana O. Salvadori. A moving boundary problem in a food material undergoing volume change - simulation of bread baking. *Food Research International*, (4):949–958, 2010.

[11] C.H. Tong and D.B. Lund. Microwave heating of baked dough products with simultaneous heat and moisture transfer. *Journal of Food Engineering*, 19(4):319–339, 1993.

[12] N. Chhanwal, D. Indrani, K. S.M.S. Raghavarao, and C. Anandharamakrishnan. Computational fluid dynamics modeling of bread baking process. *Food Research International*, 44(4):978–983, 2011.

[13] B.D. De Cindio and S. Corrers. Mathematical modeling of leavened cereal goods. *Journal of Food Engineering*, 24(3):379–403, 1995.

[14] J. Fan, J.R. Mitchell, and J.M.V. Blanshard. A model for the oven rise of dough during baking. *Journal of Food Engineering*, 41(2):69–77, 1999.

[15] B. Zanoni, C. Peri, and R. Gianotti. Determination of the thermal diffusivity of bread as a function of porosity. *Journal of Food Engineering*, 26(4):491–510, 1995.

[16] V. Jury, J. Monteau, J. Comiti, and A. Le-Bail. Determination and prediction of thermal conductivity of frozen part baked bread during thawing and baking. *Food Research International*, 40(7):874–882, 2007.

[17] Muriel J. Wagner, Lucas T., D. Le Ray, and G. Trystram. Water transport in bread during baking. *Journal of Food Engineering*, 78:1167 – 1173, 2007.

[18] Emmanuel Purlis and Viviana O. Salvadori. Modelling the browning of bread during baking. *Food Research International*, 42(7):865–870, aug 2009.

[19] J. Zhang and A.K. Datta. Some considerations in modeling moisture transport in heating hygroscopic materials. *Drying Technology*, 22(8):1983–2008, 2004.

[20] X.D. Chen and A. Putranto. *Modelling Drying Processes: A Reaction Engineering Approach*. Cambridge University Press, 2013.

[21] H. Ni and A.K. Datta. Heat and moisture transfer in baking of potato slabs. *Drying Technology*, 17(10):2069–2092, 1999.

[22] R.B. Bird, W.E. Stewart, and E.N. Lightfoot. *Transport Phenomena*. John Wiley & Sons, Inc., 2002.

[23] I. Lind and C. Rask. Sorption isotherms of mixed minced meat, dough and bread crust. *Journal of Food Engineering*, 14:303–315, 1991.

[24] COMSOL. *Multiphysics v. 5.2*. COMSOL AB, Stockholm, Sweden, 2017.

[25] S. Marc, J.P. Ploteau, P. Le-Bideau, and P. Glouannec. Transient heat flux estimation during the baking of cereal batter by contact heating. *International Journal of Heat and Mass Transfer*, 155:119848, 2020.

[26] Puvikkarasan Jayapragasam, Pascal Le Bideau, and Tahar Loulou. Approximation of heat and mass transport properties for one sided cake baking. *Journal of Food Engineering*, 290:110211, 2021.

[27] Sylwester Furmaniak, Artur P. Terzyk, Roman Gol-embiewski, Piotr A. Gauden, and Leszek Czepirski. Searching the most optimal model of water sorption on foodstuffs in the whole range of relative humidity. *Food Research International*, 42(8):1203–1214, 2009.

[28] A. Geletu. Solving optimization problems using the matlab optimization toolbox. *Personnel Note*, 2007.

[29] T.M. Le, B. Fatahi, H. Khabbaz, and W. Sun. Numerical optimization applying trust-region reflective least squares algorithm with constraints to optimize the non-linear creep parameters of soft soil. *Applied Mathematical Modelling*, 41:236–256, 2017.

[30] The MathWorks Inc. *MATLAB R2017b*. MathWorks, 3 Apple Hill Dr., Natick, MA 01760, 2017.

[31] L. Xiujuan and S. Zhongke. Overview of multiobjective optimization methods. *Journal of Systems Engineering and Electronics*, 15(2):142–146, 2004.

[32] J.N. Lyness and C.B. Moler. Numerical differentiation of analytic functions. *SIAM J. Numer. Anal.*, 4(2):202–210, 1967.

[33] P. Jayapragasam, P. Le Bideau, and T. Loulou. Computing sensitivity coefficients by using complex differentiation: Application to heat conduction problem. *Numerical Heat Transfer, Part B: Fundamentals*, 74(5):729–745, 2018.

[34] J.V. Beck and K.J. Arnold. *Parameter Estimation in Engineering and Science*. John Wiley & Sons, 1977.

[35] A.H. Feyissa, K.V. Gernaey, and J. Adler-Nissen. Uncertainty and sensitivity analysis: Mathematical model of coupled heat and mass transfer for a contact baking process. *Journal of Food Engineering*, 109(2):281–290, 2012.

[36] Halder A., Dhall A., and Datta A.K. An improved, easily implementable, porous media based model for deep-fat frying: Part i: Model development and input parameters. *Food and Bioproducts Processing*, 85(3):209–219, 2007.

[37] F.P. Incropera and D.P. DeWitt. *Fundamentals of Heat and Mass Transfer*. John Wiley & Sons, Inc., River Street, NJ, 5 edition, 2002.

A Transformation of governing equations

Moisture content U is obtained as ratio of apparent liquid density ρ_l^a to apparent solid density ρ_s^a, on dry basis.

A.1 Model I

In this model, the evaporation rate is calculated from non-equilibrium approach. By introducing the dimensionless variables, listed in table 2, the governing equations for moisture content, vapor and air are obtained as follows:

Moisture content component. Equation (1) given previously in the paper, is transformed in equation (13) by introducing U (moisture content on dry basis) is considered here for normalization as

$$\rho_s^a \frac{\partial U}{\partial t} = \nabla\left(\rho_s^a D_l \nabla U\right) - I_v \quad \Rightarrow \tag{30}$$

$$\frac{\partial U}{\partial t/t_f} = \nabla\left(D_l \times t_f/L^2 \nabla U\right) - I_v \times t_f/\rho_s^a \tag{31}$$

which it reduces to

$$\frac{\partial U}{\partial t^+} = \nabla\left(D_l^+ \nabla U\right) - I_v^+ \tag{32}$$

with the corresponding boundary conditions:

$$-D_l^+ \nabla U(x,t) = 0 \quad \text{at} \quad x = 0 \tag{33}$$

$$-D_l^+ \nabla U(x,t) = Bi_m\left(V - V^\infty\right) S_l^{S_g} \quad \text{at} \quad x = 1 \tag{34}$$

Water vapor component. Starting from initial equations (2) and (15), the normalization can be achieved in the following way:

$$\frac{\partial \pi S_g \rho_v}{\partial t} = \nabla\left(\frac{\rho_v k_g}{\mu_g} \nabla P_g\right) + \nabla\left(D \rho_{v\,g} \nabla\left(\frac{\rho_v}{\rho_g}\right)\right) + I_v \tag{35}$$

$$\frac{\partial \rho_v^a/\rho_s^a}{\partial t/t_f} = \nabla\left(\frac{\pi S_g \rho_v}{\rho_s^a} \frac{k_g t_f}{\mu_g P_{int}^g L^2} \frac{1}{\pi S_g} \nabla\left(P_g^{P_{int}^g}\right)\right) + \nabla\left(\frac{D t_f \rho_g}{L^2 \rho_s^a} \nabla\left(\frac{\rho_v^a/\rho_s^a}{\rho_g^a/\rho_s^a}\right)\right) + I_v \times t_f/\rho_s^a \tag{36}$$

which reduces to

$$\frac{\partial V}{\partial t^+} = \nabla\left(\frac{a_p^+ V}{\pi S_g} \nabla P_g^+\right) + \nabla\left(D_v^+ G \nabla\left(\frac{V}{G}\right)\right) + I_v^+ \tag{37}$$

and the boundary condition are given by:

$$-\frac{a_p^+ V(x,t)}{\pi S_g} \nabla P_g^+(x,t) - D_v^+ G(x,t) \nabla \frac{V(x,t)}{G(x,t)} = 0 \quad \text{at} \quad x = 0 \tag{38}$$

$$-\frac{a_p^+ V(x,t)}{\pi S_g} \nabla P_g^+(x,t) - D_v^+ G(x,t) \nabla \frac{V(x,t)}{G(x,t)} = Bi_m\left(V - V^\infty\right) \quad \text{at} \quad x = 1 \tag{39}$$

Air component. Similarly to above steps, the normalization of equations (3) and (16) describing air component is obtain as follow;

$$\frac{\partial\left(\pi S_g \rho_a\right)}{\partial t} = \nabla\left(\frac{k_g}{\rho_a \mu_g} \nabla P_g\right) + \nabla\left(D \rho_{v\,g} \nabla\left(\frac{\rho_a}{\rho_g}\right)\right) \tag{40}$$

$$\frac{\partial \rho^a/\rho^a_s}{\partial t/t_f} = \nabla\left(\frac{\rho_a \pi S_g}{\rho^a_s}\frac{k_{gf}}{\mu_g P_{int} L^2 \pi S_g}\nabla\left(\frac{P_g}{P_{int}}\right)\right) + \nabla\left(\frac{D_{vf}\rho_g}{L^2}\frac{g}{\rho^a_s}\nabla\left(\frac{\rho_a/\rho^a_s}{\rho_g/\rho^a_s}\right)\right) \tag{41}$$

which it reduces to

$$\frac{\partial A}{\partial t^+} = \nabla\left(\frac{a_p^+ A}{\pi S_g}\nabla P_g^+\right) + \nabla\left(D_v^+ G \nabla\left(\frac{A}{G}\right)\right) \tag{42}$$

with the following boundary conditions

$$-\frac{a_p^+ A(x,t)}{\pi S_g}\nabla P_g^+(x,t) - D_v^+ G(x,t)\nabla\frac{A(x,t)}{G(x,t)} \quad \text{at} \quad x = 0 \tag{43}$$

$$A(x,t) = \frac{\rho_{ref}^+ \pi S_g\left(1 - P_v^+\right)}{\theta + 1} \quad \text{at} \quad x = 1 \tag{44}$$

A.2 Model II

This utilizes equilibrium approach to evaluate vapor pressure inside the medium and thus reduces number of equations used and also condense the governing equations to be solved.

Moisture content. The moisture content in model II is described by addition of mass conservation of liquid water and water vapor as:

$$\frac{\partial\left(\rho^a_s U + \rho_v \pi S_g\right)}{\partial t} + \nabla\left(n_l + n_v\right) = 0 \tag{45}$$

Since deformation effect is not considered in this work, there is no change of solid density during the baking process and taking into account the ideal gas law the above equations is written as:

$$\rho^a_s \frac{\partial U}{\partial t} + \frac{\partial\left(\pi S_g P_v\right)/\left(R_v t\right)}{\partial t} = \nabla\left(\rho^a D_{sl}\nabla U + \frac{\rho_v k_g}{\mu_g}\nabla P_g + \rho_g D_v \nabla\left(\frac{\rho_v}{\rho_g}\right)\right) \tag{46}$$

$$\rho^a_s \frac{\partial U}{\partial t} + \frac{\pi P_v}{R_v T}\frac{\partial S_g}{\partial t} - \frac{\pi P_v S_g}{R_v T^2}\frac{\partial T}{\partial t} + \frac{\pi S_g}{R_v T}\frac{\partial P_v}{\partial t} = \nabla\left(\rho^a D_{sl}\nabla U + \rho_v \frac{k_g}{\mu_g}\nabla P_g + \rho_g D_v \nabla\left(\frac{\rho_v}{\rho_g}\right)\right) \tag{47}$$

By applying necessary transformation, the precedent equation is defined in nondimensional form as:

$$\begin{aligned}
&\frac{\partial U}{\partial t^+} + \pi\frac{P_{int}}{\rho^a_s R_a T_{int}}\frac{P_v}{P_{int}}\frac{R_a}{R_v}\left(\frac{T_{int}}{T - T_{int}} + T_{int}\right)\frac{\partial S_g}{\partial t^+} \\
&- \pi\frac{S_g P_{int}}{\rho^a_s R_a T_{int}}\frac{P_v}{P_{int}}\frac{R_a}{R_v}\left(\left(\frac{T_{int}^2}{T - T_{int}}\right) + T_{int}\right)^2\frac{\partial\left(T - T_{int}\right)/T_{int}}{\partial t^+} \\
&+ \pi\frac{S_g P_{int}}{\rho^a_s R_a T_{int}}\frac{R_a}{R_v}\left(\frac{T_{int}}{T - T_{int}} + T_{int}\right)\frac{\partial P_v/P_{int}}{\partial t^+} \\
&= \nabla\left(\frac{D_{lf}t}{L^2}\nabla U + \frac{\pi S_g \rho_v}{\rho^a_s}\frac{k_{gf}t}{\mu_g L^2 P_{int}}\frac{1}{\pi S_g}\nabla P_g^+\right. \\
&\left. + \frac{P_{int}}{R_a T_{int}}\left(\frac{T_{int}}{T - T_{int}} + T_{int}\right)\left(\frac{P_g}{P_{int}} - \frac{P_v}{P_{int}}\right)\left(1 - R_a/R_v\right)\right) \\
&\times \frac{D_v \times t_f}{L^2}\nabla\frac{\left(\left(P_g/P_{int}\right)/\left(1/P_v/P_{int} - 1\right)R_a/R_v\right)/}{\partial}
\end{aligned} \tag{48}$$

In the above equation ∇ operator corresponds to $\frac{}{\partial(x/L)}$ and after introducing some nondimensional numbers,

$$\begin{aligned}
&\frac{\partial U}{\partial t^+} + \frac{\pi\rho^+_{ref} P^+_v}{\left(\theta + 1\right)R^+_v}\frac{\partial S_g}{\partial t^+} - \frac{\pi S_g \rho^+_{ref} P^+_v}{\theta + 1}\frac{\partial\theta}{\partial t^+} + \frac{\pi S_g \rho^+_{ref}}{R^+_v\left(\theta + 1\right)}\frac{\partial P^+_v}{\partial t^+} \\
&= \nabla\left(D_l^+\nabla U + \frac{a_p^+ V}{\pi S_g}\nabla P_g^+ + \frac{\rho_{ref}}{\theta + 1}\left(P_g^+ - P_v^+\left(1 - 1/R_v^+\right)\right)D_v^+\nabla\left(\frac{1}{1 + P_g^+/P_v^+ - 1/R_v^+}\right)\right)
\end{aligned} \tag{49}$$

Γ^+

with the following boundary conditions

$$\Gamma^{+}(x, t) = 0 \qquad x = 0 \tag{50}$$

$$\Gamma^{+}(x, t) = Bi_m \left(V - V^{\infty}\right) \qquad x = 1 \tag{51}$$

Total gas pressure. For total gas pressure P_g is obtained from mass conservation of air with help of Dalton's law of partial pressure ($P_g = P_v + P_a$) as following,

$$\frac{\partial}{\partial t}\left(\pi S_g \left(\rho_g - \rho_v\right)\right) + \nabla n_a = 0 \tag{52}$$

Using ideal gas law and some algebraic transformations, we obtain

$$\begin{aligned}
&\frac{\pi S_g}{R_a T}\frac{\partial P_g}{\partial t} - \frac{\pi S_g P_g}{R_a T^2}\frac{\partial T}{\partial t} + \frac{\pi P_g}{R_a T}\frac{\partial S_g}{\partial t} - \frac{\pi S_g}{R_a T}\frac{\partial P_v}{\partial t} + \frac{\pi S_g P_v}{R_a T^2}\frac{\partial T}{\partial t} - \frac{\pi P_v}{R_a T}\frac{\partial S_g}{\partial t} \\
&\quad = \nabla\left(\frac{k_g\left(P_g - P_v\right)}{\mu_g R_a T}\nabla P_g\right) - \nabla\left(\frac{1}{T}\left(\frac{P_v}{R_v} + \frac{P_g - P_v}{R_a}\right) D_v \nabla\left(\frac{1}{1 + \left(P_g - P_v\right)R_v / \left(P_v R_a\right)}\right)\right)
\end{aligned} \tag{53}$$

$$\begin{aligned}
&\pi\frac{S_g P_{int}}{R_a T_{int}}\left(\frac{T_{int}}{T - T_{int}} + T_{int}\right)\frac{\partial P_g / P_{int}}{\partial t / t_f} - \pi\frac{S_g P_{int}}{R_a T_{int}}\left(\frac{T_{int}}{T - T_{int}} + T_{int}\right)\frac{\partial P_v / P_{int}}{\partial t / t_f} \\
&\quad + \pi\frac{P_{int}}{R_a T_{int}}\frac{P_g - P_v}{P_{int}}\left(\frac{T_{int}}{T - T_{int}} + T_{int}\right)\frac{\partial S_g}{\partial t / t_f} \\
&\quad - \pi\frac{S_g P_{int}}{R_a T_{int}}\frac{P_g - P_v}{P_{int}}\left(\frac{T_{int}^2}{\left(T - T_{int}\right)^2 + T_{int}}\right)\frac{\partial\left(T - T_{int}\right)/T_{int}}{\partial t / t_f} \\
&\quad = \nabla\Phi^{+}
\end{aligned} \tag{54}$$

where the analytic expression of variable Φ^{+} is given by:

$$\begin{aligned}
\Phi^{+} &= \frac{P_g - P_v\left(1 - R_a / R_v\right)}{P_{int}}\frac{P_{int}}{R_a T_{int}}\left(\frac{T_{int}}{T - T_{int}} + T_{int}\right)\frac{D_v t_f}{L^2} \\
&\quad \times \nabla\left(\frac{1}{1 + \left(\frac{P_g}{P_{int}} \times \frac{P_{int}}{P_v} - 1\right)R_v / R_a}\right) \\
&\quad - \frac{P_{int}}{R_a T_{int}}\frac{P_g - P_v}{P_{int}}\left(\frac{T_{int}}{T - T_{int}} + T_{int}\right)\frac{k_g t_f}{\mu_g L^2 P_{int}}\nabla\left(\frac{P_g}{P_{int}}\right)
\end{aligned} \tag{55}$$

Finally the nondimensional form is written as:

$$\frac{\pi S_g \rho_{ref\_g}}{\theta - 1}\frac{\partial P^{+}}{\partial t^{+}} + \frac{\pi\left(P_g^{+} - P_v^{+}\right)\rho_{ref}}{\theta + 1}\frac{\partial S_g}{\partial t^{+}} - \frac{\pi\left(P_g^{+} - P_v^{+}\right)S_g\rho_{ref}}{\left(\theta + 1\right)^2}\frac{\partial\theta}{\partial t^{+}} - \frac{\pi S_g \rho_{ref}}{\theta + 1}\frac{\partial P_v^{+}}{\partial t^{+}} = \nabla\Phi^{+} \tag{56}$$

and the analytic expression of variable Φ^{+} is given by:

$$\Phi^{+} = \frac{\left(P_g^{+} - P_v^{+}\right)\left(1 - 1/R_v\right)\rho_{ref\,v} + D^{+}}{\theta + 1}\nabla\left(\frac{1}{1 + P_g^{+}/P_v^{+} - 1 R_v^{+}}\right) - \frac{\left(P_g^{+} - P^{+}\right) + a^{+}}{\theta + 1}\rho_{ref\,v}\nabla P_g^{+} \tag{57}$$

with the following boundary conditions:

$$\Phi^{+}(x, t) = 0 \qquad \text{at} \qquad x = 0 \tag{58}$$

$$P_g^{+}(x, t) = 0 \qquad \text{at} \qquad x = 1 \tag{59}$$

List of Tables

		Model I	Model II
Energy conservation		$\frac{\partial\theta}{\partial t^+} = a_q^+\nabla^2\theta - R_l I_v^+$	
Mass conservation	Liquid water	$\frac{\partial U}{\partial t^+} = \nabla\left(D_l^+\nabla U\right) - I_v^+$	$\frac{\partial U}{\partial t^+} + \left(\frac{\pi\rho_{ref}^+}{1+\theta R_v^+}\right) P_v^+\frac{\partial S_g}{\partial t^+} - S_g P^+\frac{\partial\theta}{\partial t^+} + S_g\frac{\partial P_v^+}{\partial t^+} = \nabla\Gamma$
	Water vapor	$\frac{\partial V}{\partial t^+} = \nabla\left(\frac{a_p^+ V}{\pi S_g}\nabla P_g^+\right) + \nabla\left(D_v^+ G\nabla\frac{V}{G}\right) + I_v^+$	$\frac{\pi\rho_{ref}^+}{1+\theta} S_g\frac{\partial P_g^+}{\partial t^+} + \frac{P_g^+ - P_v^+}{1+\theta}\frac{\partial S_g}{\partial t^+} - S_g\frac{\partial\theta}{\partial t^+} - S_g\frac{\partial P_v^+}{\partial t^+} = \nabla\Phi$
	Air	$\frac{\partial A}{\partial t^+} = \nabla\left(\frac{a_p^+ A}{\pi S_g}\nabla P_g^+\right) + \nabla\left(D_v^+ G\nabla\frac{A}{G}\right)$	
Boundary conditions			
Heat transfer	$x = 0$	$-\nabla\theta = Q k^+$	
	$x = 1$	$-\nabla\theta = Bi_q k^+\left(\theta(1,t^+) - \theta^\infty\right)$	
Mass transfer (liquid)	$x = 0$	$\nabla U = 0$	$\Gamma = 0$ (for explanation refer to mass conservation of liquid water)
	$x = 1$	$-D_l^+\nabla U = Bi_m S_l S_g(V - V^\infty)$	$\Gamma = Bi_m(V - V^\infty)$
Mass transfer (gases)	$x = 0$	$\frac{a_p^+ V}{\pi S_g}\nabla P_g^+ + D_v^+ G\nabla\left(\frac{V}{G}\right) = 0$ for vapor	$\Phi = 0$ (for explanation refer to mass conservation of gaseous phase)
		$\frac{\partial A}{\partial t^+} = \nabla\left(\frac{a_p^+ A}{\pi S_g}\nabla P_g^+\right) + \nabla\left(D_v^+ G\nabla\frac{A}{G}\right)$ for air	
Mass transfer (gases)	$x = 1$	$\frac{a_p^+ V}{\pi S_g}\nabla P_g^+ + D_v^+ G\nabla\frac{V}{G} = Bi_m\left(V - V^\infty\right)$ for vapor	$P_g^+ = 0$
		$A = \frac{\rho_{ref}^+\,\pi S_g\left(1 - P_v^+\right)}{1+\theta}$ for air	
Closure term			
Evaporation rate I_v^+		$H^+\left(V^{eq} - V\right)$	from conservation of water vapor

Table 1: Governing equations for model I and II in nondimensional form. The analytic expression of Γ and Φ are given below in the text.

$\theta = \frac{T - T_0}{T_0}$	$a_q^+ = \frac{a_q t_f}{L^2}$	$R_l = \frac{\rho_s^a \lambda}{\rho_{eff} c_{p_{eff}} T_0}$	$I_v^+ = \frac{I_v t_f}{\rho_s^a}$	$Q = \frac{qL}{k_{ref} T_0}$
$k^+ = \frac{k_{ref}}{k}$	$Bi_q = \frac{h_q L}{k_{ref}}$	$\theta^\infty = \frac{T^\infty - T_0}{T_0}$	$U = \frac{\rho_l^a}{\rho_s^a}$	$D_l^+ = \frac{D_l t_f}{L^2}$
$\rho_{ref}^+ = \frac{P_0}{R_a T_0 \rho_s^a}$	$R_v^+ = \frac{R_v}{R_a}$	$P_v^+ = \frac{P_v}{P_0}$	$V = \frac{\rho_v^a}{\rho_s^a}$	$a_p^+ = \frac{k_g t_f P_0}{\mu_g L^2}$
$P_g^+ = \frac{P_g}{P_0}$	$D_v^+ = \frac{D_v t_f}{L^2}$	$Bi_m = \frac{h_m t_f}{L}$	$V^\infty = \frac{\rho_v^\infty}{\rho_s^a}$	$A = \frac{\rho_a^a}{\rho_s^a}$
$G = A + V$	$H^+ = H \times t_f$	$V^{eq} = \frac{\rho^{eq}}{\rho_s^a}$	$t^+ = \frac{t}{t_f}$	$x^+ = \frac{x}{L}$

Table 2: Non-dimensional parameters

Parameters	Expression/Values	Units	Description
Bi_m	$\frac{Bi_q}{\rho c_p^a L_e^{2/3}\left(L^2/k_{ref}t_f\right)}$	–	From boundary layer theory [37].
a_w	$\frac{0.99}{\exp\left(0.042\,U^{-1.11}\right)}$	–	Water activity
R_l	$\frac{\lambda}{\rho C_p}\frac{\rho_s^a}{T_{int}}$	–	Calculated from known variables
ρc_p	$\frac{k_{ref}}{k^+}\frac{t_f}{a_q^+ L^2}$	–	Calculated from known variables
q	$31000t^{-0.33}$	W/m^2	Applied heat flux (experimental)
λ	2.5×10^6	J/kg	Latent heat ofvaporization
μ_g	1.8×10^{-5}	$Pa \cdot s$	Dynamic viscosity for gas
k_g	1.2×10^{-14}	m^2	Calculated as average from function $k_g^i \times k_g^r$
π	0.76	–	Porosity (calculated)
S_0	0.9	–	Liquid Saturation initial (calculated)
U_0	1.6	–	Moisture content initial
T_0	296	K	Initial temperature
P_0	101325	Pa	Initial Pressure
T^∞	294	K	Ambient temperature
RH	25.0	%	Relative Humidity of surrounding
ρ_v^∞	0.0046	kg/m^3	Ambient vapor density
k_{ref}	1	$W/m \cdot K$	Reference thermal conductivity
L	0.008	m	Overall length
t_f	1200	s	Baking period, final time
ρ_s^a	436	kg/m^3	Apparent solid density (calculated)
$\rho\, c_{p_{eff}}$	4185	$kJ/m^3 \cdot K$	Effective volumetric heat capacity
k_{eff}	0.3125	$W/m \cdot K$	Effective thermal conductivity
h_q	10	$W/m^2 \cdot K$	Convective heat transfer coefficient
h_m	...	m/s	Convective mass transfer coefficient
D_l	4.96×10^{-10}	m^2/s	Effective mass diffusivity for liquid water
D_v	1.234×10^{-6}	m^2/s	Effective mass diffusivity for water vapor
H	10	1/s	Evaporation rate constant
a_p^+	1284	–	Capillarity diffusivity
a_q^+	1.4	–	Thermal diffusivity
Bi_q	0.080	–	Biot heat number
D_l^+	0.0093	–	Liquid water diffusivity
D_v^+	23.125	–	Vapor diffusivity
H^+	12000	–	Evaporation rate constant
k^+	3.2	–	Thermal conductivity

Table 3: Thermophysical data and resulting dimensionless parameters used in the simulation

	a_q^+	D_w^+	D_v^+	H^+	k^+	Bi_q
a_q^+	1.00	0.63	−0.01	−0.16	0.89	−0.50
D_I^+		1.00	−0.36	−0.40	0.55	−0.79
D_v^+			1.00	0.59	0.04	0.76
H^+				1.00	−0.27	0.37
k^+					1.00	−0.31
Bi_q						1.00

(a) - Model I

	a_q^+	D_w^+	D_v^+	Bi_q	k^+
a_q^+	1.00	0.94	−0.83	0.23	0.93
D_I^+		1.00	−0.89	0.19	0.93
D_v^+			1.00	0.16	−0.80
Bi_q				1.00	0.29
k^+					1.00

(b) - Model II

Table 4: Correlation matrix of dimensionless parameters for model I and II

Model	Parameter	Exact v. $\varphi' \rightarrow$	Without noise ($\sigma = 0$)			With noise ($\sigma \neq 0$)		
			0.4	0.5	0.6	0.4	0.5	0.6
I	a_q^+	1.5173	1.33	2.03	1.21	12.47	9.61	2.20
	Bi_q	0.096	9.67	14.68	9.35	37.84	27.86	3.28
	D_I^+	0.028125	22.79	32.49	23.13	66.67	66.67	40.38
	D_v^+	28.125	18.51	28.57	18.43	65.39	58.15	36.25
	H^+	11496	2.92	5.16	3.09	137.16	56.55	12.49
	k^+	3.2287	0.77	1.17	0.73	14.61	12.72	4.72
II	a_q^+	1.3554	0.37	0.08	0.88	4.5	3.34	1.87
	Bi_q	0.048	0.06	0.64	7.29	14.89	12.40	7.36
	D_I^+	0.01875	0.62	0.78	7.82	11.63	15.42	16.19
	D_v^+	28.125	3.71	1.35	1.33	7.96	13.03	18.01
	k^+	3.125	0.01	0.10	4.03	11.31	10.49	8.55

Table 5: Overview of percentage error in estimating dimensionless parameters with simulated measurements (without noise and with noise) for model I and II and for different values of weighting factor φ

Model	Parameters	Initial guess	Weighting factor φ		
			0.4	0.5	0.6
I	a_q^+	0.08	1.9737	2.0354	1.6328
	Bi_q	0.03	0.093591	0.093592	0.096
	D_w^+	0.009	0.067397	0.07033	0.14833
	D_v^+	9.00	70.071	12.892	281.14
	H^+	120.0	12882	34546	2328.9
	k^+	0.60	2.6682	2.592	2.9585
II	a_q^+	0.08	1.3139	1.3722	1.3654
	Bi_q	0.03	0.07934	0.072213	0.067889
	D_w^+	0.009	0.015496	0.013776	0.012463
	D_v^+	9.00	24.455	19.24	19.414
	k^+	0.60	3.3255	3.1651	3.389

Table 6: Estimated nondimensional parameters for model I and II as function of weighting factor φ using experimental data

Weighting factor φ	Temperature sensor			Mean moisture content
	Tc_3	Tc_4	Tc_6	
0.4	2.78×10^{-2}	1.66×10^{-2}	1.44×10^{-2}	2.95×10^{-2}
0.5	3.30×10^{-2}	2.12×10^{-2}	2.43×10^{-2}	3.21×10^{-2}
0.6	1.48×10^{-2}	1.97×10^{-2}	1.24×10^{-2}	2.88×10^{-2}

(a) - Model I

Weighting factor φ	Temperature sensor			Mean moisture content
	Tc_3	Tc_4	Tc_6	
0.4	3.80×10^{-2}	1.24×10^{-2}	2.01×10^{-2}	8.43×10^{-3}
0.5	3.69×10^{-2}	1.55×10^{-2}	1.29×10^{-2}	6.95×10^{-3}
0.6	3.68×10^{-2}	1.66×10^{-2}	1.19×10^{-2}	5.71×10^{-3}

(b) - Model II

Table 7: Root mean square values for temperature and mean moisture content for model I and II obtained with experimental data. The rms values for temperature are displayed for each sensor location.

Parameters	Units	Model-I	Model-II
k_{eff}	$W/m \cdot K$	0.338	0.30
$\rho c_{p_{eff}}$	$MJ/m^3 \cdot K$	3.88	4.05
D_w	$(\times 10^3)\ mm^2/s$	7.91	0.67
D_v	mm^2/s	15.1	1.04
H	1/s	1.94	– –
h_q	$W/m^2 \cdot K$	12.00	8.48
h_m	m/s	0.0117	0.0082

Table 8: Estimated physical parameters with experimental data for both model I and II. The weighting factor was set to $\varphi = 0.6$

List of Figures

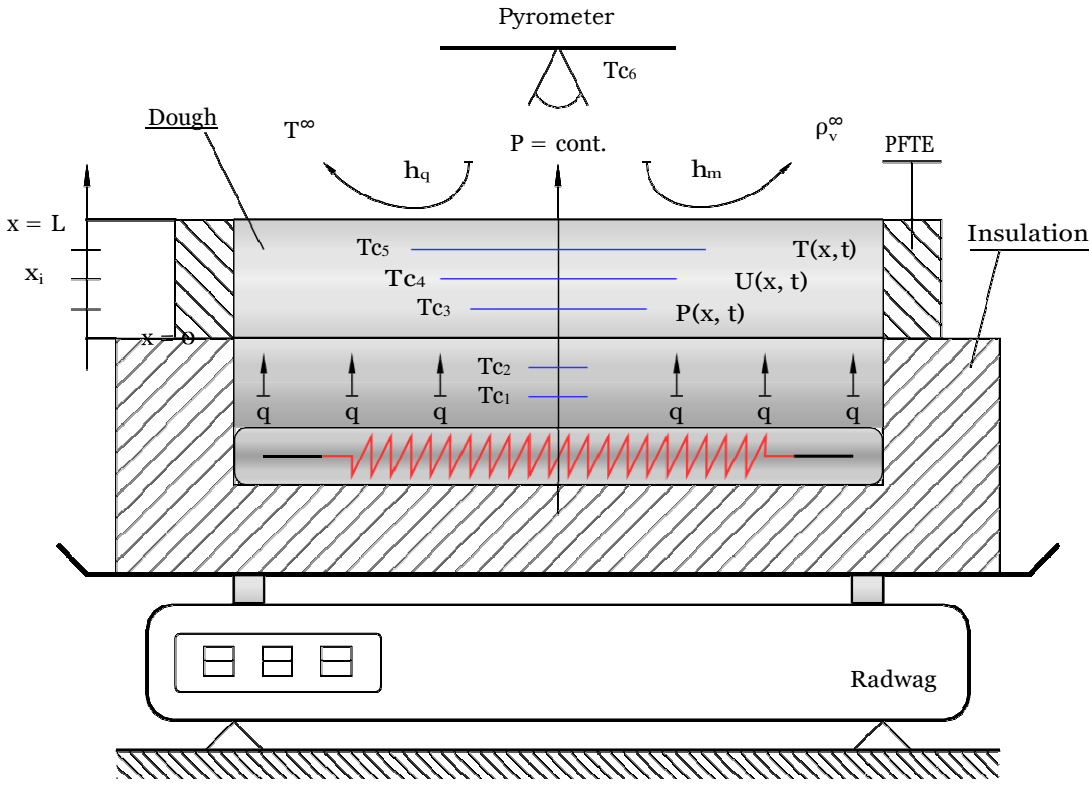

Figure 1: Experimental setup, coordinates, boundary conditions and geometry of the model.

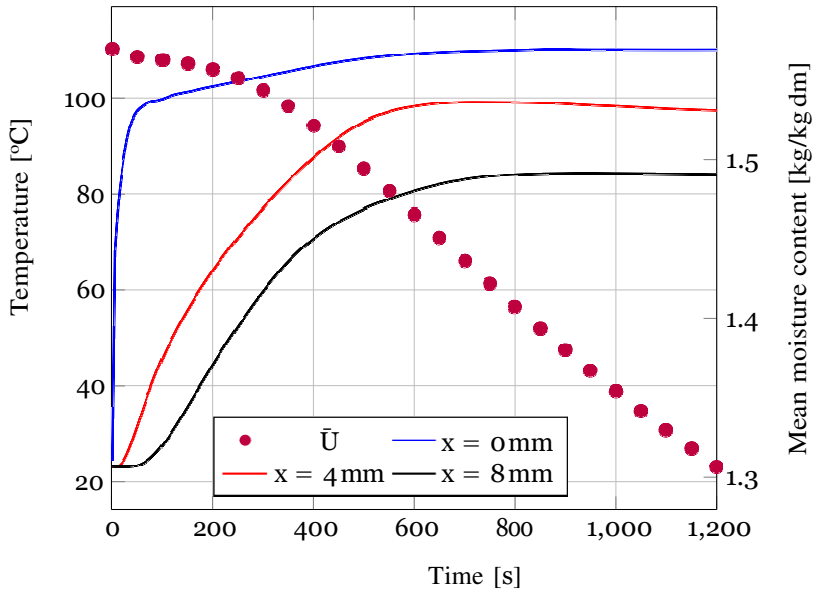

Figure 2: Simulated temperature and mean moisture content during the baking process

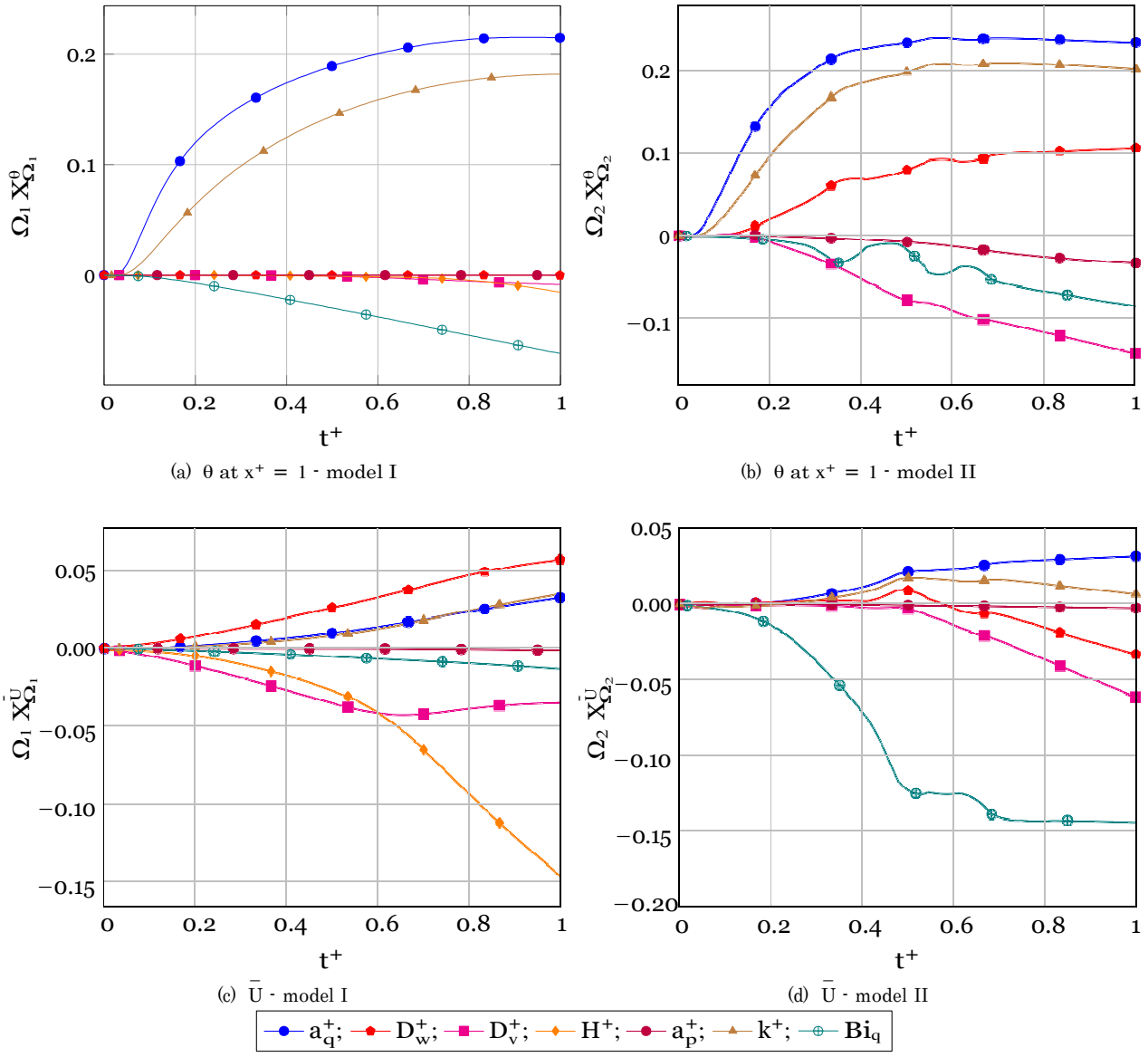

(a) θ at $x^+ = 1$ - model I

(b) θ at $x^+ = 1$ - model II

(c) $\bar{U}$ - model I

(d) $\bar{U}$ - model II

Figure 3: Scaled sensitivity profiles for temperature at $x^+ = 1$ and mean moisture content for model I (figures a and c) and model II (figures b and d)

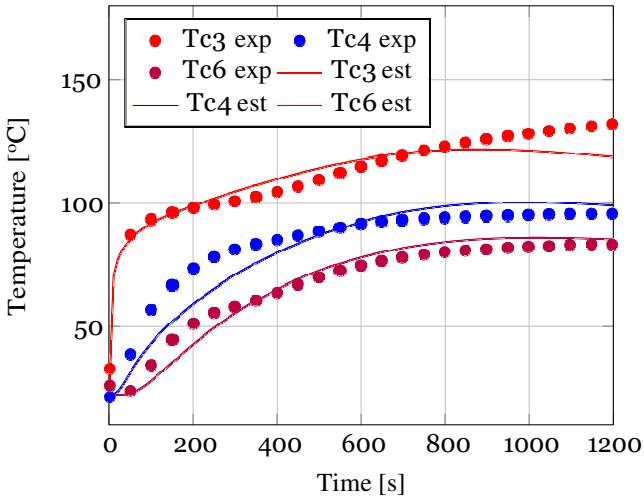

(a) Temperature

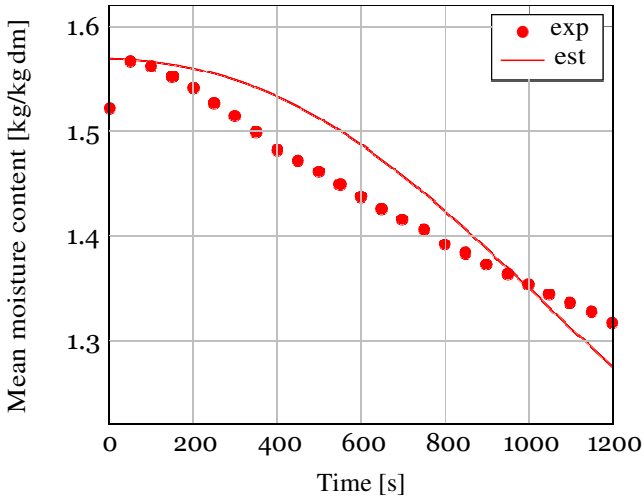

(b) Mean moisture content

Figure 4: Experimental measurements and simulated results of temperature (a) and mean moisture content (b) for model I with weight $\varphi = 0.6$ (where exp - experimental measurements, est - estimated results)

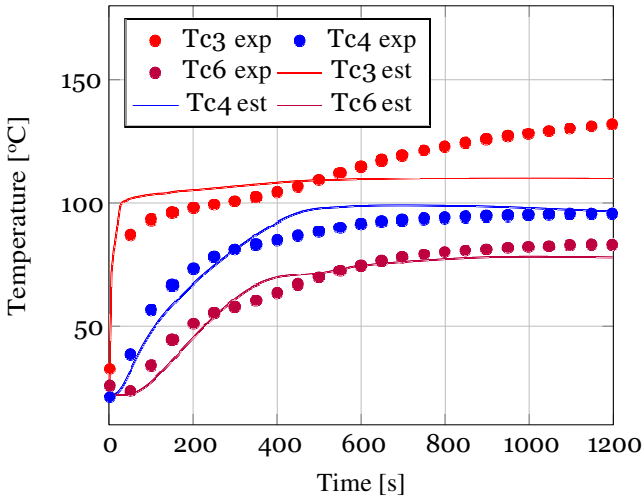

(a) Temperature

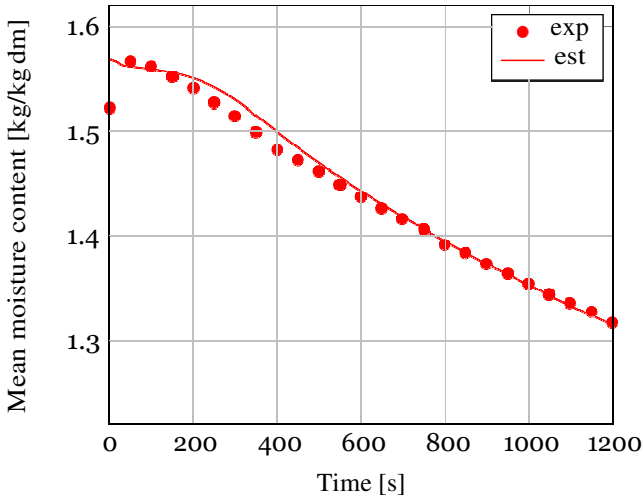

(b) Mean moisture content

Figure 5: Experimental measurements and simulated results of temperature (a) and mean moisture content (b) for model II with weight $\varphi = 0.6$ (where exp - experimental measurements, est - estimated results)

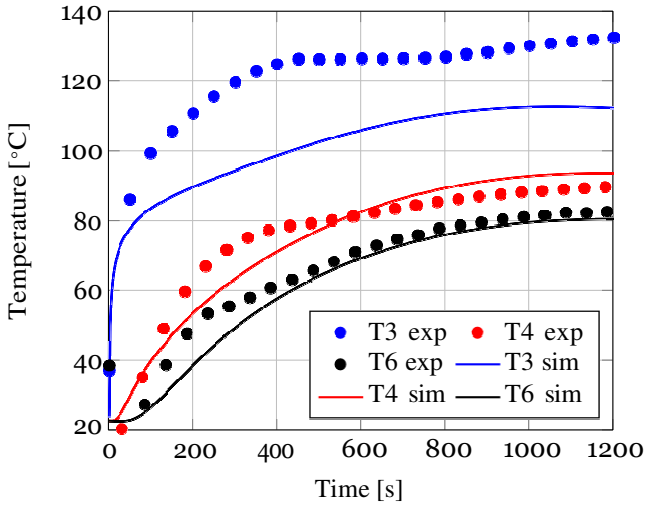

(a) Temperature - model I

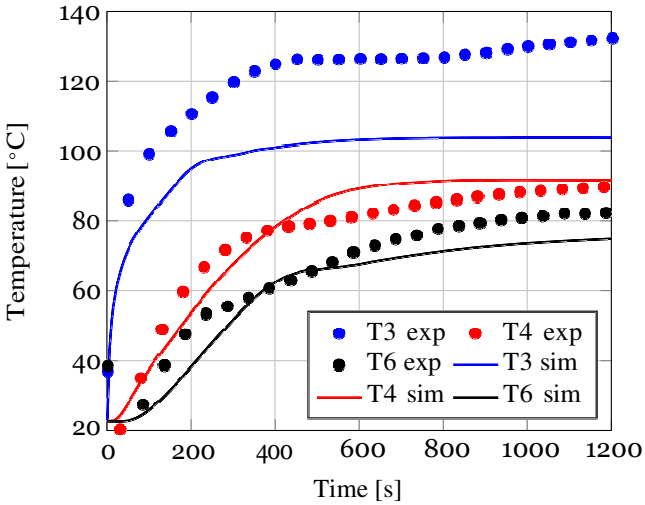

(b) Temperature - model II

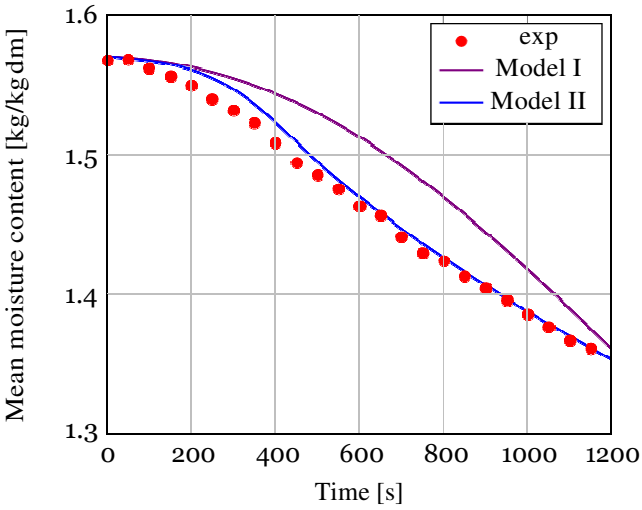

(c) Mean moisture content

Figure 6: Experimental measurements and simulated results of model I and model II for regulator temperature 170°C (where exp is experimental data and sim is simulated results)

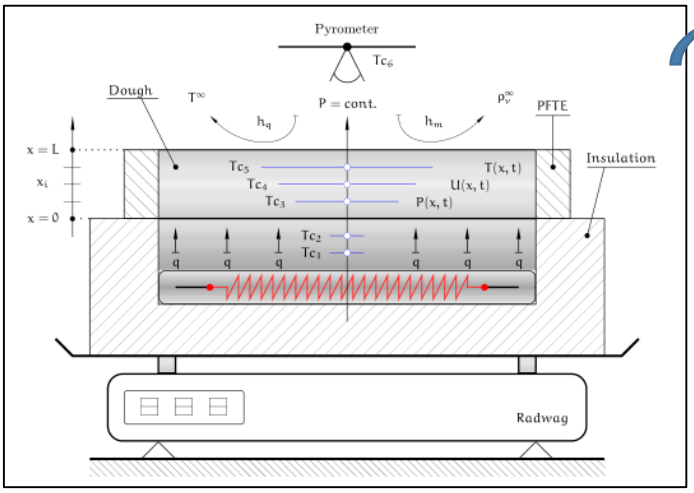

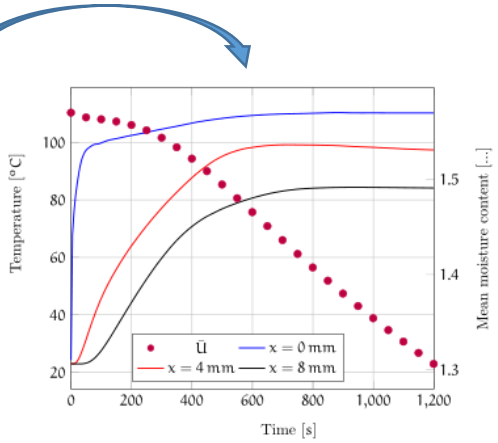

Optimization Tools

Estimation of thermophysical properties